Mergos, P.E. & Kappos, A. J. (2013). Analytical study on the influence of distributed beam vertical loading on seismic response of frame structures. Earthquake and Structures, 5(2), pp. 239-259.

CITY UNIVERSITY LONDON

City Research Online

Analytical study on the influence of distributed beam vertical loading on seismic response of frame structures

P.E. Mergos[*1a] and A.J. Kappos[1b]

[1]*City University London, School of Engineering and Mathematical Sciences, Department of Civil Engineering, London EC1V 0HB, United Kingdom*

Abstract. Typically, beams that form part of structural systems are subjected to vertical distributed loading along their length. Distributed loading affects moment and shear distribution, and consequently spread of inelasticity, along the beam length. However, the finite element models developed so far for seismic analysis of frame structures either ignore the effect of vertical distributed loading on spread of inelasticity or consider it in an approximate manner. In this paper, a beam-type finite element is developed, which is capable of considering accurately the effect of uniform distributed loading on spreading of inelastic deformations along the beam length. The proposed model consists of two gradual spread inelasticity sub-elements accounting explicitly for inelastic flexural and shear response. Following this approach, the effect of distributed loading on spreading of inelastic flexural and shear deformations is properly taken into account. The finite element is implemented in the seismic analysis of reinforced concrete (R/C) frame structures with beam members controlled either by flexure or shear. It is shown that to obtain accurate results the influence of distributed beam loading on spreading of inelastic deformations should be taken into account in the inelastic seismic analysis of frame structures.

Keywords: seismic analysis; finite element; distributed inelasticity; beam members; distributed loading.

1. Introduction

In recent years, nonlinear analysis procedures, although more complex and computationally demanding, have gained favour over the conventional linear elastic methods for the seismic analysis of structures. This is the case because they model realistically structural response and provide reliable and accurate analytical predictions. Nevertheless, the inherent assumptions of these procedures may, in some cases, jeopardize their credibility and drive the analysis to erroneous results.

It is well known that beam members are subjected to distributed vertical loading along their length. Beam distributed loading arises from the supported slab area distributed loads, the overlying infill walls, and beam self-weight. Distributed loading generates nonlinear bending moment diagrams and variation of the acting shear forces along the member length.

In the vast majority of inelastic seismic analyses, beam distributed loading is either ignored or treated in an approximate manner. Typically, end-moments arising from distributed loading are added to the seismic end-moments, but the moment diagram is assumed to be linear and the acting shear force constant along the beam length. This approach originates from the assumption that under a strong earthquake, distributed

[*] Corresponding author: Lecturer, E-mail: panmerg@yahoo.com
[a] Lecturer. E-mail: panmerg@yahoo.com
[b] Professor. E-mail: Andreas.Kappos.1@city.ac.uk

loading moments and shears represent a negligible fraction of the respective seismic demand. However, this is not the actual situation in a number of cases arising in real structures. This is particularly the case in buildings with long-span beams and/or heavy slabs and infill walls, and in all buildings subjected to low seismic actions, especially in their upper floors. The significance of accurately modelling the effect of distributed beam loading on spreading of inelastic flexural and shear deformations increases if one considers the fact that capacity design principles, adopted by all modern seismic design guidelines, dictate development of plastic hinges at the beam ends, so that a beam-sway mechanism develops and a soft-storey mechanism is prevented.

The above remarks point to the need for a finite element capable of consistently modelling distributed beam loading effects in inelastic seismic analysis of structures. A large number of finite element models of the beam-column type have been proposed for inelastic seismic analysis of frame structures. The most common and widely used ones are the concentrated (lumped) plasticity models (Clough and Johnston 1966; Giberson 1967). These models, while computationally attractive, may yield inaccurate predictions because the assumed inelastic zone length is in reality a function of the boundary conditions and member moment distribution (Anagnostopoulos 1981).

In recent years, flexural force-based distributed finite elements (Spacone et al. 1996; Neuenhofer and Filippou 1997) have gained favour, because this approach provides fairly accurate prediction of inelastic response with a single element discretization of the structural member. Moreover, a number of these elements have been enhanced to account for shear flexibility (Ceresa et al. 2007). Nevertheless, distributed inelasticity elements using Gauss or Gauss-Lobatto integration techniques are not computationally efficient for members with inelastic deformations only at their ends (Lee and Filippou 2009), as the case typically is with seismic loading. In this case, the aforementioned finite elements behave like an element with an inelastic zone of fixed length at each end, if only the integration point closest to the end of the member experiences yielding (Lee and Filippou 2009). The length of the inelastic zone equals the integration weight of the end monitoring section. Increasing the number of integration points is computationally inefficient, unless the element is subdivided into an inelastic region at each end and an intermediate elastic region (Addessi and Ciampi 2007). Even so, it is possible that only the integration point closest to the end experiences plastic deformations, particularly for small strain hardening ratios (Lee and Filippou 2009).

Lee and Filippou (2009) compared the performance of conventional distributed inelasticity force-based elements applying the Gauss-Lobatto integration technique and that of a new finite element with variable inelastic end-zones (named SIZE model) proposed in their study. They found that under double curvature conditions (typical case under seismic loading), the distributed inelasticity element with 5 fixed integration points may lead to significant deviations from the exact solution. On the other hand, the SIZE model was found to provide very good convergence with less computational cost. To achieve the same level of accuracy, 10 equal-length finite elements with 5 Gauss-Lobatto integration points were applied by these researchers for the structural member under investigation.

When distributed vertical loading is present, the problem of capturing the spread of inelasticity by conventional distributed inelasticity elements, with fixed monitoring sections, becomes less significant for sagging moments, but it becomes more important for hogging moments. This is the case because, when distributed loading is

present, the bending moment diagram decreases from the support to the mid-span more rapidly in the hogging moment region and less rapidly in the sagging moment region, compared to the case that there is no distributed loading (which is never true for beams). Hence, for the same end moments (controlled by the member's flexural capacity), the length of the inelastic end zone becomes smaller for hogging moments and larger for sagging moments with respect to the zero distributed loading case. As a result, the possibility that only the integration point closest to the end experiences plastic deformations increases for the end with hogging moment and decreases for the end with sagging moment. Both these effects of distributed vertical loading are further explained in the remainder of the paper.

Furthermore, for these conventional distributed inelasticity elements incorporating shear flexibility, the lengths of the flexural and shear inelastic end regions are restricted to be identical and equal to the integration weight of the monitoring section. Hence, the possibility that the inelastic flexural and shear deformations expand along different lengths due to the different moment and shear force variation along the structural member cannot be modelled explicitly by these elements.

To capture the gradual spreading of inelastic deformations, a spread inelasticity formulation with variable length inelastic zones is needed. Several research studies have introduced such flexural inelasticity elements. Meyer et al. (1983), Reinhorn et al. (2009), Lee and Filippou (2009) and Roh et al. (2012) proposed flexural gradual spread inelasticity models, which ignore influence of distributed loading. Soleimani et al. (1979) and Filippou and Issa (1988) suggested similar flexural spread inelasticity beam models, where distributed loading is taken into account approximately by assuming constant shear force in the plastic hinge regions. Kyakula and Wilkinson (2004) proposed a flexural spread plasticity model, where the inelastic zones ends are determined by linear interpolation between fixed monitoring sections, where differences between acting and yielding moments change sign. This approach may take into account the influence of distributed loading. Nevertheless, it is an approximate method and it may require a significant number of monitoring sections.

None of the aforementioned gradual spread inelasticity elements, apart from the model of Roh et al. (2012), considers variation of shear flexibility along beam members.

Mergos and Kappos (2009, 2012) developed a shear spread inelasticity model to capture shear-flexure interaction effect for R/C members with constant shear force. The model assumes inelastic shear end zones with variable length defined by the respective zones of the flexural sub-element. A similar approach has been adopted by Roh et al. (2012).

Furthermore, in an earlier work (Mergos and Kappos 2008), the authors introduced the concept of a shear spread plasticity model which captures variation of shear flexibility, when distributed loading is present and acting shear varies along the member length. However, since this analytical work focussed on shear-flexure interaction of single R/C column members, the complete formulation of the proposed model to account for the beam distributed loading effect on spreading of both inelastic flexural and shear deformations was not developed. Moreover, the analytical model was not applied in seismic analysis of beam members with distributed loading.

The main goal of the present study is to investigate the influence of beam vertical distributed loading on seismic response of frame structures. To this purpose, a new flexural and shear gradual spread inelasticity beam finite element for inelastic seismic analysis of plane frame structures is presented. The proposed model is developed for the special case of uniform distributed loading. However, it is straightforward to be

extended to cope with different types of vertical loading. The analytical model formulation is described in detail, together with its inherent assumptions. Finally, the analytical model is implemented in a computer code for inelastic static and dynamic analysis and applied to plane frames with different configurations. Useful conclusions are drawn regarding the influence of beam vertical loading on seismic response of R/C frame structures.

2. Finite Element Model Formulation

2.1 General description

The proposed, member-type, finite element is based on the flexibility approach (force-based element) and belongs to the class of phenomenological models. It consists of two sub-elements representing flexural and shear element response (see Fig. 1). The total flexibility matrix [F] is calculated as the sum of the flexibilities of its sub-elements and can be inverted to produce the element stiffness matrix [K]; hence:

$$[F] = [F^{fl}] + [F^{sh}] \tag{1}$$

where, [F], [F^{fl}], [F^{sh}] are the basic total, flexural, and shear, respectively, tangent flexibility matrices. [K] is the basic tangent stiffness matrix of the element, relating incremental moments ΔM_A, ΔM_B and rotations $\Delta\theta_A$, $\Delta\theta_B$ at the ends A and B of the flexible part of the element (Fig. 1).

The flexural sub-element is used for modelling flexural behaviour of the beam member subjected to cyclic loading before, as well as after, flexural yielding. It consists of a set of rules governing the hysteretic moment-curvature (M-φ) behaviour of the member end sections, and the flexural spread plasticity model. The flexural spread plasticity model is composed of the model for flexural stiffness distribution and the model for determination of the variable length of the inelastic flexural end-zones.

The shear sub-element is defined in the same way as its flexural counterpart. It is determined by a set of rules governing the hysteretic shear force vs. shear distortion (V-γ) behaviour of the member end sections and the shear spread plasticity model; the latter is composed of the model for shear stiffness distribution and the model for defining the variable length of the inelastic shear end-zones.

Due to their similarity, the individual components of the flexural and shear sub-elements are developed in parallel in the following sections. Analytical model assumptions and limitations are also discussed.

Closing this general description, it is worth noting that additional sub-elements may be added in series to the afore-described formulation in order to account for other sources of flexibility. This may be the case, for example, for the fixed-end rotations developing at the R/C beam-column interfaces due to anchorage slippage in the neighbouring joint regions (Mergos and Kappos 2009, 2012).

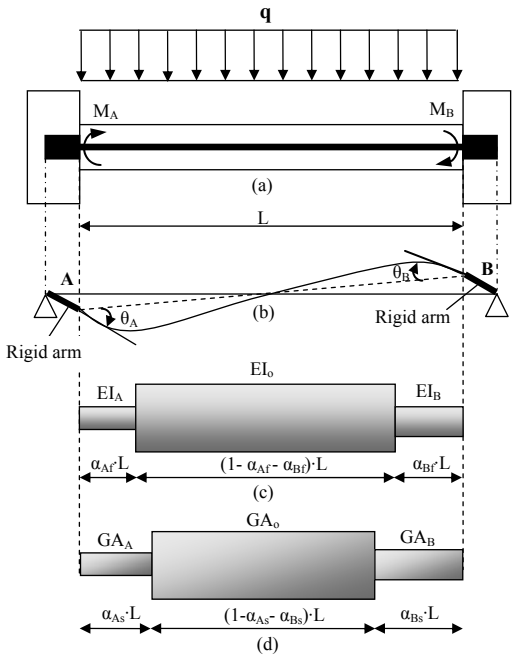

Figure 1: Proposed finite element model: a) geometry of R/C beam member with distributed vertical loading; b) beam finite element with rigid offsets; c) flexural sub-element; d) shear sub-element

2.2 End-section hysteretic relationships

An appropriate M-φ and V-γ hysteretic model is applied to determine the hysteretic response of end-sections of the flexural and shear sub-element, respectively. These hysteretic models are described by the primary (skeleton) curve and the rules determining section response under cyclic loading.

In this study, it is assumed that envelope M-φ and V-γ responses can be adequately approximated by a bilinear skeleton curve (Fig. 2). This skeleton curve consists of an elastic and a post-elastic linear branch separated at the level of flexural M_y or shear yielding V_y. Furthermore, it is assumed herein that shear yielding is independent of flexural yielding and vice versa. The latter assumption may not be accurate for some classes of structural members like for example shear-flexure critical RC members (Mergos and Kappos 2012). Nevertheless, for the vast majority of structural members, especially those designed according to modern seismic design principles, shear-flexure interaction maybe disregarded with reasonable accuracy (Lehman and Moehle 1998; Beyer et al. 2011).

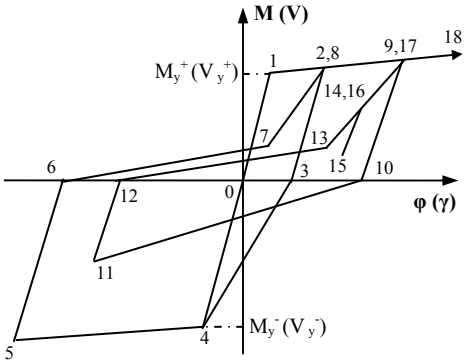

Figure 2: M-φ (V-γ) sub-element end-section hysteretic models

The multi-linear, 'yield-oriented' with slip, hysteretic model of Sivaselvan and Reinhorn (2000) is adopted herein for describing M-φ and V-γ cyclic behaviour. This model accounts for stiffness degradation, strength deterioration, pinching effect and non-symmetric response. However, its original formulation is based on a trilinear envelope curve. Hence, its hysteretic rules were appropriately modified by the authors (Mergos and Kappos 2008) to make them compatible with a bilinear skeleton curve. In general, different hysteretic parameters are applied to describe hysteretic flexural and shear response.

2.3 Stiffness distribution

To capture the current distribution of section flexural and shear stiffness along the beam, a gradual flexural and shear, respectively, spread inelasticity model is assigned (Soleimani et al. 1979; Mergos and Kappos 2008, 2012). Following this model, each sub-element is divided into two inelastic end-regions and one elastic intermediate zone.

Inelastic end-zones determine the part of the flexural or shear sub-element where flexural or shear yielding, respectively, have occurred. The length of these inelastic zones generally varies throughout member response and the way it is defined at each analysis step is described in the following sections.

Stiffness along the intermediate zone is assumed to be constant and equal to the elastic stiffness EI_o of the end-section M-φ envelope curve for the flexural sub-element and GA_o of the end-section V-γ envelope curve for the shear sub-element. If the elastic stiffnesses of the two end-sections are different, then an average value is assigned to the intermediate zone (Eq. 2) as also suggested by Reinhorn et al. (2009), where EI_{oA}, EI_{oB}, GA_{oA}, GA_{oB} are the elastic stiffnesses at the ends A and B respectively.

$$EI_o = \frac{2 \cdot EI_{oA} \cdot EI_{oB}}{EI_{oA} + EI_{oB}} \; ; \; GA_o = \frac{2 \cdot GA_{oA} \cdot GA_{oB}}{GA_{oA} + GA_{oB}} \tag{2}$$

Stiffness distribution within the inelastic zones depends on the loading state of the end section hysteretic response. In particular, Fig. 3 illustrates hysteretic response of four cross-sections located inside one region of the flexural (shear) sub-element. It can be seen that when all sections remain on the strain hardening branch (loading state), flexural (shear) stiffness remains constant in the inelastic zone and equal to $r \cdot EI_o$ ($r \cdot GA_o$) ($0<r<1$).

However, when the end sections are in the unloading and reloading state, stiffness varies from a minimum value $r_1 \cdot EI_o$ ($r_1 \cdot GA_o$) and $r_2 \cdot EI_o$ ($r_2 \cdot GA_o$) ($0<r_1,r_2<1$) corresponding to the end section, to a maximum value, which is equal to EI_o (GA_o). Hence, under the general assumption that the loading state of all sections of the yielded region remains the same, it can be considered that when M-φ (V-γ) end section hysteretic response is on the strain hardening branch, stiffness distribution remains uniform in the inelastic zone. In the case where end-section M-φ (V-γ) behaviour is in the unloading or reloading state, it is assumed that the stiffness varies linearly from end section flexural (shear) stiffness to their elastic counterparts.

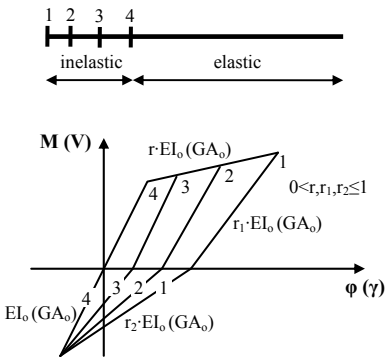

Figure 3. M-φ (V-γ) hysteretic response of cross-sections inside a plastic hinge

In line with the previous observations, stiffness distribution along the member may be assumed to have one of the shapes shown in Fig. 4, where L is the length of the member; EI_o (GA_o) is the stiffness in the intermediate part of the element and EI_A (GA_A) and EI_B (GA_B) are the current tangent flexural (shear) rigidities of the sections at the ends A and B respectively. The flexural (shear) rigidities EI_A (GA_A) and EI_B (GA_B) are determined by the M-φ (V-γ) hysteretic relationships of the corresponding end sections. Similar assumptions are made by Soleimani et al. (1979) and Roh et al. (2012).

Nevertheless, it should be kept in mind that these assumptions remain a compromise between the need for low computational cost, as assured by the use of only two monitoring end-sections, and the need for accurate representation of the stiffness distribution along the member length. The validity of these assumptions increases as the length of the inelastic zones decreases (Soleimani et al. 1979). Hence, for the typical cases of seismic response, where the lengths of the inelastic zones remain relatively small, the aforementioned assumptions are deemed as adequate.

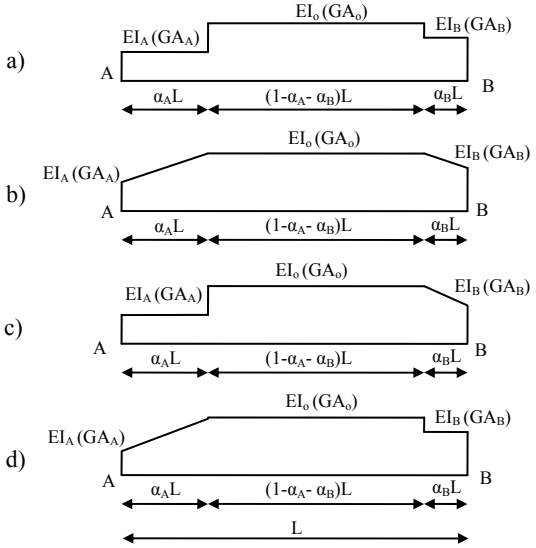

Figure. 4. Element stiffness distribution: (a) when ends A and B are in the loading state; (b) when ends A and B are both in the unloading or reloading state; (c) when end A is in the loading and end B is in the unloading or reloading state; (d) when end A is in the unloading or reloading state and end B is in the loading state

2.4 Inelastic end-zone lengths

In Fig. 4, α_A and α_B are the inelastic zone coefficients. The inelastic zone coefficients specify the proportion of the member that has yielded either in flexure (α_{Af} and α_{Bf}) or in shear (α_{As} and α_{Bs}). By definition, α_{Af} and α_{Bf} represent the part of the flexural sub-element, where acting moment exceeds section yield moment and α_{As} and α_{Bs} represent the part of the shear sub-element, where acting shear exceeds shear yielding capacity.

It is known that due to the presence of uniform distributed loading, the moment diagram becomes parabolic, while shear force varies linearly along the beam length. Fig. 5 illustrates the determination of moment and shear inelastic zone lengths for a beam member subjected to uniform distributed loading, when end-moments (shears) have opposite signs. It is noted that the moment and shear force distributions shown in this figure do not correspond to the same loading condition of the beam member; they are grouped together herein simply because the same methodology can be applied for the determination of their corresponding inelastic zone coefficients. In Fig. 5a, it can be seen that for sagging moments the actual inelastic zone lengths may be significantly underestimated and for hogging moments they may be seriously overestimated, when parabolic moment distribution is not taken into account.

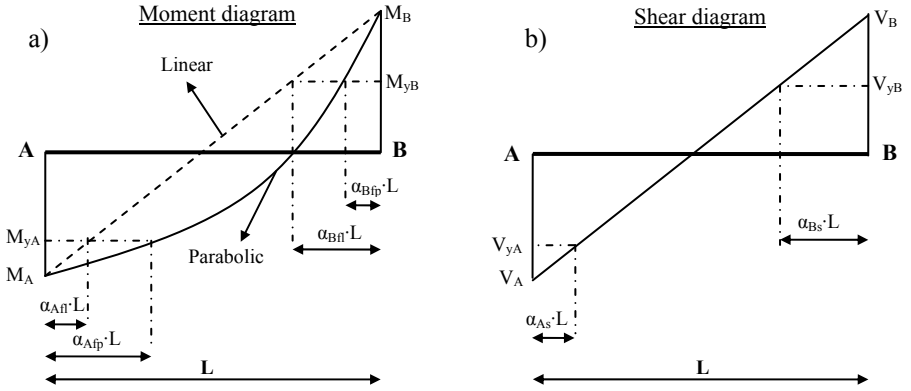

Figure 5. Determination of inelastic end-zone lengths when end-moments (shears) have different signs: (a) flexural sub-element; (b) shear sub-element

When end-moments (shears) have different signs, inelastic zone lengths may be determined by the location of the moment (shear) distribution, where acting moment (shear) becomes equal to the respective end-section yield moments (M_{yA}, M_{yB}) or shears (V_{yA}, V_{yB}). Hence, the flexural yielding penetration coefficients α_{Afp} and α_{Bfp}, which take into consideration nonlinear moment distribution, are given by Eq. (3), where $q>0$ is the value of the uniform distributed loading and shear forces V_A and V_B are given by Eq. (4).

$$\alpha_{Afp} = \frac{V_A \pm \sqrt{V_A^2 - 2q \cdot \left(M_{yA} - M_A\right)}}{q \cdot L} \le 1 \; ; \; \alpha_{Bfp} = \frac{-V_B \pm \sqrt{V_B^2 - 2q \cdot \left(M_{yB} - M_B\right)}}{q \cdot L} \le 1 \qquad (3)$$

$$V_A = \frac{q \cdot L}{2} + \frac{M_B - M_A}{L} \; ; \; V_B = -\frac{q \cdot L}{2} + \frac{M_B - M_A}{L} \qquad (4)$$

It is noted that, when end-moments have opposite signs (Fig. 5a), Eq. (3) provides always a unique solution in the range [0, 1], when end-moments exceed the respective end-section yield moments.

It is also worth noting that, in some cases (e.g. variation of longitudinal reinforcement along R/C beam members), the yielding moments in the interior of the structural member may be different from the respective values at its end sections. This issue can be easily resolved by solving Eq. (3) for the different yield moment values and selecting the unique solution of the inelastic zone coefficient, which lies in the range of the respective yield moment.

For the calculation of the shear yielding coefficients α_{As} and α_{Bs}, Eq. (5) holds. It is worth noting that the same equation provides the solution for the flexural yielding coefficients α_{Afl} and α_{Bfl}, when linear distribution is assumed, if the shear forces are substituted by the respective bending moments. Eqs. (3) and (5) are valid for both sagging and hogging moments as long as the absolute values of the acting moments (shears) are greater than their yielding counterparts. In these equations, the yield moments (shears) must be introduced with the same signs as the respective acting values.

$$\alpha_{As} = \frac{V_A - V_{Ay}}{V_A - V_B}\ ;\ \alpha_{Bs} = \frac{V_B - V_{By}}{V_B - V_A} \tag{5}$$

Fig. 6 illustrates the determination of moment and shear inelastic zone lengths for a beam member subjected to uniform distributed loading, when end-moments (shears) have the same sign; the figure presents the case, where only one member end (end A) yields.

It is noted that Fig. 6a does not represent the typical scenario for bending moments under seismic loading, but it is addressed herein since it is required for the generality of the analytical solution. Again, it can be seen that for hogging moments the actual inelastic zone lengths may be significantly overestimated when parabolic moment distribution is not taken into account.

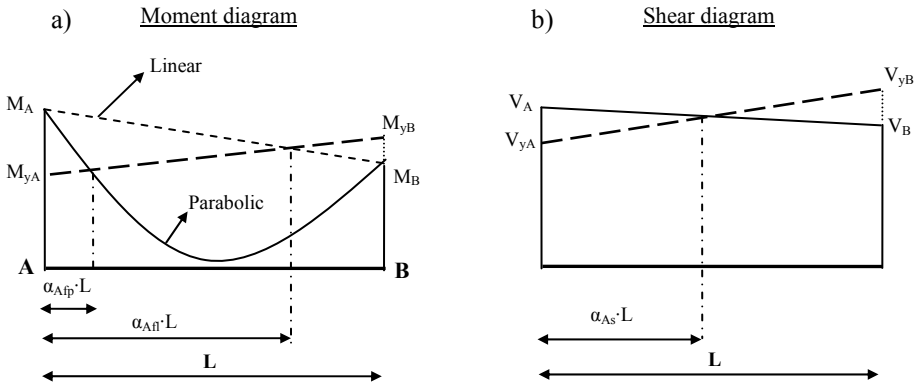

Figure 6. Determination of inelastic end-zone lengths when end-moments (shears) have same signs: (a) flexural sub-element; (b) shear sub-element.

When end-moments (shears) have same signs, inelastic zone lengths may reach high values (Fig. 6b). Hence, it is proposed herein that they are determined by the location of the moment (shear) distribution, where acting moment (shear) meets the line connecting end-section yield moments, as shown in Fig. 6. Under this assumption, the flexural inelastic zone coefficients α_{Afp} and α_{Bfp} are given by Eq. (6), where values $V_{A,eq}$ and $V_{B,eq}$ are given by Eq. (7). It is noted that Eq. (6) applies only to the member ends, where acting moments exceed the corresponding yield moments.

$$\alpha_{Afp} = \frac{V_{A,eq} \pm \sqrt{V_{A,eq}^2 - 2q \cdot \left(M_{yA} - M_A\right)}}{q \cdot L};\ \alpha_{Bfp} = \frac{-V_{B,eq} \pm \sqrt{V_{B,eq}^2 - 2q \cdot \left(M_{yB} - M_B\right)}}{q \cdot L} \quad (6)$$

$$V_{A,eq} = V_A - \frac{M_{yB} - M_{yA}}{L};\ V_{B,eq} = V_B - \frac{M_{yB} - M_{yA}}{L}; \quad (7)$$

Similarly, for the shear yielding coefficients α_{As} and α_{Bs}, Eq. (8) holds, which provides also the solution for the flexural yielding coefficients α_{Afl} and α_{Bfl}, by substituting shear forces with the corresponding bending moments.

$$\alpha_{As} = \frac{V_A - V_{yA}}{V_A - V_{yA} + V_{yB} - V_B};\ \alpha_{Bs} = \frac{V_B - V_{yB}}{V_B - V_{yB} + V_{yA} - V_A} \quad (8)$$

When one acting end-moment (shear) is higher than the respective value at yield while the other is not, then Eqs. (6 to 8) provide unique solutions in the range [0, 1]. Furthermore, for the case of sagging parabolic moments and linearly distributed shear forces, if both end-moments (shears) are higher than their yield counterparts, then the entire moment (shear) diagram exceeds the line connecting the yield values of the member ends. Consequently, the entire beam member can be considered to be 'yielded'. For these cases, following the suggestions of Reinhorn et al. (2009), it is assumed that

$$\alpha_{Af} = 0.5;\ \alpha_{Bf} = 0.5;\ \alpha_{As} = 0.5;\ \alpha_{Bs} = 0.5;\ EI_o = \frac{2 \cdot EI_A \cdot EI_B}{EI_A + EI_B};\ GA_o = \frac{2 \cdot GA_A \cdot GA_B}{GA_A + GA_B} \quad (9)$$

For hogging parabolic moments, if both end-moments are higher than their yield values, then two cases may arise: Eq. (6) has either two or no solutions in the range [0, 1]. In the first case, the solution providing the lower value of the inelastic zone lengths α_{Afp} and α_{Bfp} is adopted. In the second case, the complete member is considered as having yielded and Eq. (9) is applied.

In all cases, inelastic zone coefficients are first calculated for the current moment (shear) distribution. Then, they are compared with their previous maximum values; inelastic zone coefficients cannot be smaller than their previous maxima (Soleimani et al. 1979; Reinhorn et al. 2009). Moreover, special measures are taken to adjust flexibility distribution of members, when the sum of the two inelastic zone coefficients at the member ends exceeds unity ($\alpha_A + \alpha_B > 1$). In such cases, the elastic stiffness EI_o (GA_o) is properly modified to capture actual flexibility distribution (Reinhorn et al. 2009).

Finally, Fig. 7 illustrates the development of an internal flexural inelastic zone. In this case, yielding of an interior part of the beam member occurs prior to yielding of the member ends. The formulation of the proposed element model does not address this case, for several reasons. First, this situation is highly unlikely to develop (although the shape of this moment diagram is quite common at early stages of the response), since in most cases hinges form due to seismic loading, at the member ends. Second, for beam members dominated by gravity loading, seismic loading is not critical and does not contribute significantly to the bending moments in the mid-span. Moreover, hysteretic response of the internal inelastic zone cannot be properly captured by the hysteretic behaviour of the member end-sections. Monitoring hysteretic behaviour of several cross sections along the member length is typically required, which increases considerably the computational cost. However, this removes the main advantages of the proposed model, which are simplicity, transparency, and efficiency. Hence, for the

cases where internal hinges are expected, e.g. in analysis considering the vertical component of the earthquake, it is proposed herein that the beam member is divided into a sufficient number of finite elements. In most cases this can be omitted, since these members are not the critical ones in the assessment of the structure.

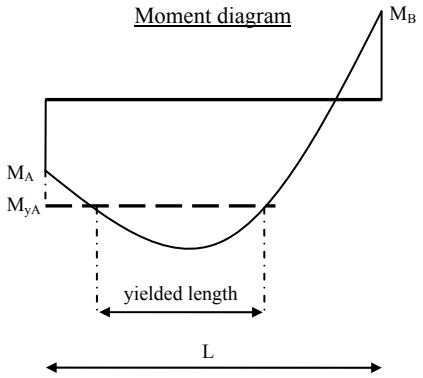

Figure. 7. Development of internal inelastic zone

2.5 Flexibility coefficients

Having established the flexural and shear stiffness distributions along the beam member at each step of the analysis, the coefficients of the flexibility matrix of the flexural and shear sub-element can be derived by applying the principle of virtual work.

For the flexural flexibility coefficients, the general Equation (10) holds, where $m_i(x)$ and $m_j(x)$ are the moment distributions due to a virtual unit end moment at end A and B respectively, and EI(x) is the tangent flexural stiffness distribution along the beam member.

$$f_{ij}^{fl} = \int_0^L \frac{m_i(x) \cdot m_j(x)}{EI(x)} dx \quad (i,j=A,B) \tag{10}$$

For the stiffness distributions shown in Fig. 4, Eq. (10) yields the closed-form solution of Eq. (11), where the parameters c_o, c_A, c_B are defined in Table 1.

$$f_{ij}^{fl} = \frac{L}{12EI_o}\left(c_o + c_A \cdot \gamma_A + c_B \cdot \gamma_B\right) = \frac{L}{12EI_o} \cdot \varphi_{ij}^{fl};\ \gamma_A = \frac{EI_o}{EI_A} - 1;\ \gamma_B = \frac{EI_o}{EI_B} - 1 \tag{11}$$

For the shear flexibility coefficients, the general Eq. (12) holds, where $v_i(x)$ and $v_j(x)$ are the shear distributions due to a virtual unit end moment at end A and B respectively, and GA(x) is the tangent shear stiffness distribution along the beam member.

$$f_{ij}^{sh} = \int_0^L \frac{v_i(x) \cdot v_j(x)}{GA(x)} dx \quad (i,j=A,B) \tag{12}$$

It can be shown that for the stiffness distributions shown in Fig. 4, Eq. (12) yields the closed-form solution of Eq. (13), where the parameters d_o, d_A, d_B are defined in Table 1.

$$f_{ij}^{sh} = \frac{1}{GA_o \cdot L}\left(d_o + d_A \cdot \delta_A + d_B \cdot \delta_B\right) = \frac{1}{GA_o \cdot L} \cdot \varphi_{ij}^{sh};\ \delta_A = \frac{GA_o}{GA_A} - 1;\ \delta_B = \frac{GA_o}{GA_B} - 1 \tag{13}$$

Fig. 8 illustrates the variation of the normalized flexural flexibility coefficients φ^{fl}_{ii} and φ^{fl}_{ij} ($i \neq j$) with the flexural inelastic zone coefficients for the typical range of

values developed under seismic loading $0 \leq \alpha_i, \alpha_j \leq 0.25$ (Filippou and Issa 1988). It is assumed that the stiffness distribution is uniform in the inelastic zones and that the ratio of the post elastic to the elastic flexural stiffness is equal to 1%. Two limit cases are examined. In the first case, the yielding penetration coefficient of the j section is equal to zero and in the second case it is equal to 0.25. The strong dependence of the flexibility matrix coefficients from the inelastic zone coefficients is evident. This observation emphasizes the need for accurate simulation of the spread of inelasticity.

Table 1. Determination of flexural and shear flexibility matrix coefficient parameters

Flexibility coefficient	Stiffness distribution	c_o	c_A	c_B	d_o	d_A	d_B
f_{AA}	Fig. 4a	4	$12\alpha_{Af}-12\alpha_{Af}^2+4\alpha_{Af}^3$	$4\alpha_{Bf}^3$	1	α_{As}	α_{Bs}
f_{BB}	Fig. 4a	4	$4\alpha_{Af}^3$	$12\alpha_{Bf}-12\alpha_{Bf}^2+4\alpha_{Bf}^3$	1	α_{As}	α_{Bs}
f_{AB}	Fig. 4a	-2	$4\alpha_{Af}^3-6\alpha_{Af}^2$	$4\alpha_{Bf}^3-6\alpha_{Bf}^2$	1	α_{As}	α_{Bs}
f_{AA}	Fig. 4b	4	$6\alpha_{Af}-4\alpha_{Af}^2+\alpha_{Af}^3$	α_{Bf}^3	1	$\alpha_{As}/2$	$\alpha_{Bs}/2$
f_{BB}	Fig. 4b	4	α_{Af}^3	$6\alpha_{Bf}-4\alpha_{Bf}^2+\alpha_{Bf}^3$	1	$\alpha_{As}/2$	$\alpha_{Bs}/2$
f_{AB}	Fig. 4b	-2	$\alpha_{Af}^3-2\alpha_{Af}^2$	$\alpha_{Bf}^3-2\alpha_{Bf}^2$	1	$\alpha_{As}/2$	$\alpha_{Bs}/2$
f_{AA}	Fig. 4c	4	$12\alpha_{Af}-12\alpha_{Af}^2+4\alpha_{Af}^3$	α_{Bf}^3	1	α_{As}	$\alpha_{Bs}/2$
f_{BB}	Fig. 4c	4	$4\alpha_{Af}^3$	$6\alpha_{Bf}-4\alpha_{Bf}^2+\alpha_{Bf}^3$	1	α_{As}	$\alpha_{Bs}/2$
f_{AB}	Fig. 4c	-2	$4\alpha_{Af}^3-6\alpha_{Af}^2$	$\alpha_{Bf}^3-2\alpha_{Bf}^2$	1	α_{As}	$\alpha_{Bs}/2$
f_{AA}	Fig. 4d	4	$6\alpha_{Af}-4\alpha_{Af}^2+\alpha_{Af}^3$	$4\alpha_{Bf}^3$	1	$\alpha_{As}/2$	α_{Bs}
f_{BB}	Fig. 4d	4	α_{Af}^3	$12\alpha_{Bf}-12\alpha_{Bf}^2+4\alpha_{Bf}^3$	1	$\alpha_{As}/2$	α_{Bs}
f_{AB}	Fig. 4d	-2	$\alpha_{Af}^3-2\alpha_{Af}^2$	$4\alpha_{Bf}^3-6\alpha_{Bf}^2$	1	$\alpha_{As}/2$	α_{Bs}

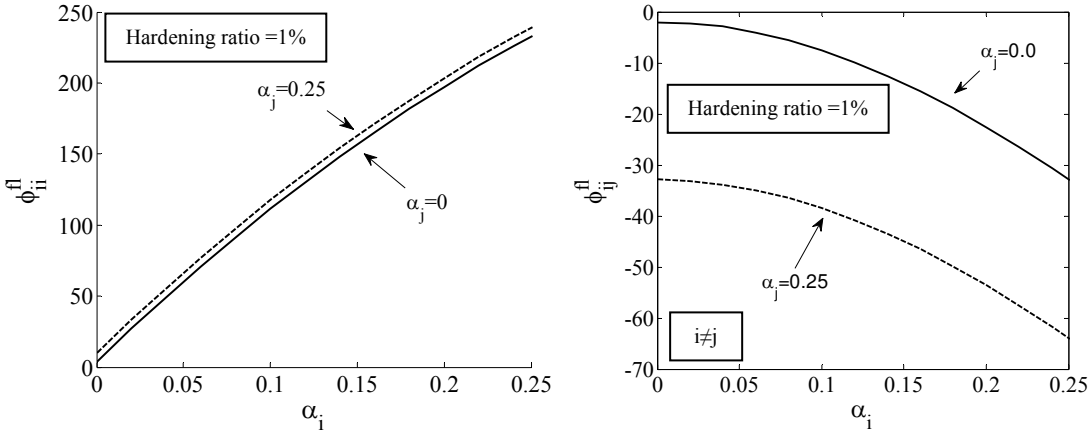

Figure 8. Variation of the normalized flexural flexibility matrix coefficients with the yielding penetration coefficients for hardening ratio 1% and uniform stiffness distribution in the inelastic zones.

3. Numerical model validation

In this section, the proposed numerical model is validated against the analytical solutions provided in Anagnostopoulos (1981) for prismatic beam members whose cross section response can be adequately represented by a bilinear M-φ curve (with hardening ratio r) in monotonic loading (Fig. 2). Shear flexibility is ignored in both the numerical and the analytical solutions.

In the analytical study by Anagnostopoulos (1981), beam loading consists of two end rotation increments (Fig. 1) $\Delta\theta_A$ and $\Delta\theta_B$ (differences between maximum and yield rotations) with ratio $\Delta\theta_A/\Delta\theta_B=n$. It is also assumed that before these rotations are applied, the member is bent by two end moments M_A and M_B where $M_A=c\cdot M_y$ and $M_B=M_y$. M_y is the common yield moment of both end sections, assumed the same in positive and negative bending. The imposed end rotations are assumed to act with or without the presence of a uniform distributed loading q, superimposing a bending moment $M_G=q\cdot L^2/8$ in the middle of the beam member.
The analytical solutions provide the post-yield secant stiffness ratios S_i (i=A,B) as a function of the imposed rotation ductility demands $\mu_{\theta i}$ for both member ends. The post-yield secant stiffness ratios are defined as

$$S_i = \frac{\left(\frac{\Delta M_i}{\Delta \theta_i}\right)}{K_i} \tag{14}$$

where ΔM_i is the moment increment at end i (difference between maximum and yield moment) and K_i is the elastic stiffness, which is equal to $6EI_o/L$ for n=1 (antisymmetric bending).
In the following, the analytical solutions will be compared with the results of the proposed numerical model for the following conditions: n=1, c=1, r=0.05. Regarding beam distributed loading q, two separate cases are examined: $M_G=0$ (i.e. q=0) and $M_G=0.5M_y$.
To simulate the above conditions, a symmetric beam member with properties $EI_o=10^4$kNm^2, $M_y=10^3$kNm, $\varphi_y=10^{-1}$m^{-1}, L=10m, r=0.05 and q=0 or q=40kN/m, was subjected to pushover analysis using the proposed finite element model.
Fig. 9 compares the predicted S_i values as a function of the imposed $\mu_{\theta i}$ by the proposed numerical model and the analytical solutions by Anagnostopoulos (1981). Circles represent some discrete results of the analytical solutions (obtained by the use of special software for digitizing graphical data) and the continuous lines the predictions of the proposed numerical model. It is seen that the matching between the two solutions is excellent.

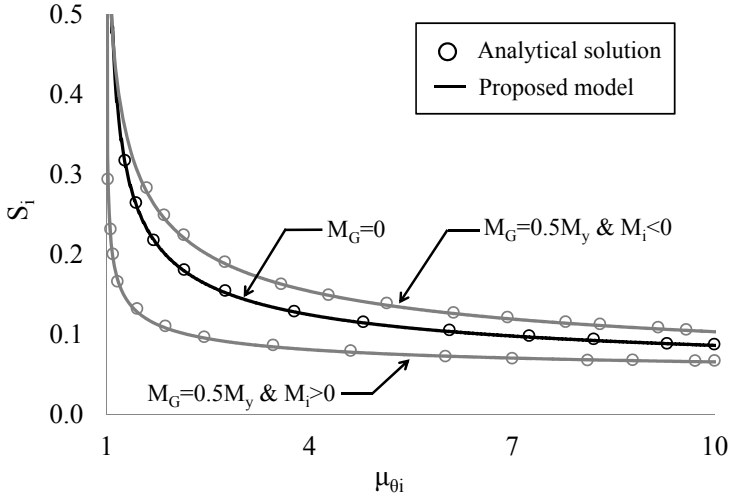

Figure 9. Comparison of the calculated post-yield secant stiffness ratios as a function of the imposed rotation ductility derived by the proposed numerical model and the analytical solutions by Anagnostopoulos (1981)

It is important to note that post-yield secant stiffness decreases faster with $\mu_{\theta i}$ for sagging moments ($M_i>0$) than for hogging moments, when distributed beam loading q is present. This occurs because the length of the inelastic zone is greater for the member end with the sagging moment for the same value of ΔM_i. The solution without distributed loading lies between the solutions for sagging and hogging moments, when distributed loading is applied. All curves tend to $S_i=1$ for $\mu_{\theta i}=1$.

4. Numerical model implementation

The proposed member-type model is implemented in a computer program (IDARC2D) for the nonlinear dynamic analysis of R/C structures (Reinhorn et al. 2009). It is then used for the inelastic static and dynamic analyses of plane frame structures with beam members dominated either by flexure or shear. In these analyses, the column members are modelled by the existing column element of IDARC2D, which accounts for axial flexibility and it is accurate for linear moment diagrams. In addition to the above, parametric analyses are conducted in order to investigate the influence of beam gravity loading on inelastic seismic response of frame structures.

4.1 R/C Frame structure with flexure dominated beam members

The six-storey frame examined herein is part of an R/C building designed according to EC8 for a ground acceleration of 0.36g. The materials used in the structure are C25/30 (characteristic cylinder strength of 25 MPa) concrete and B500c steel (characteristic yield strength of 500 MPa). The total dead and live loads on the floor slabs are assumed to be 6.5kN/m^2 and 2.0kN/m^2, respectively. In addition, infill walls represented by linear distributed loads 10kN/m are present on the first four storeys of the frame. Frame layout, vertical loads for the seismic combination and cross-section details are presented in Fig. 10. It is noted that due to the application of capacity design principles, only flexural yielding is expected to be developed for the beam members of the frame.

To investigate the importance of distributed loading, three different models are set up for the inelastic seismic analysis of this frame. Model 1 assumes a constant hinge length equal to $0.08L_s$, where L_s is the member shear span; L_s is taken equal to L/2 for all beam and column members; this is a reasonable average value within the range resulting during the response to seismic loading. Anchorage slip effect is not included in this study, in order to obtain a clearer picture of the effect of gravity loading on spreading of inelasticity. Model 2 employs a gradual spread inelasticity element, but distributed beam loading effect is not considered for the calculation of the inelastic end-zone lengths (i.e. moment diagram is assumed to be linear). Finally, model 3, which is the one proposed in this study, takes into account distributed beam loading effects in a consistent manner. All models consider nodal moments arising from beam distributed loading. During inelastic analyses described later on, no internal flexural inelastic zones developed in the beam members.

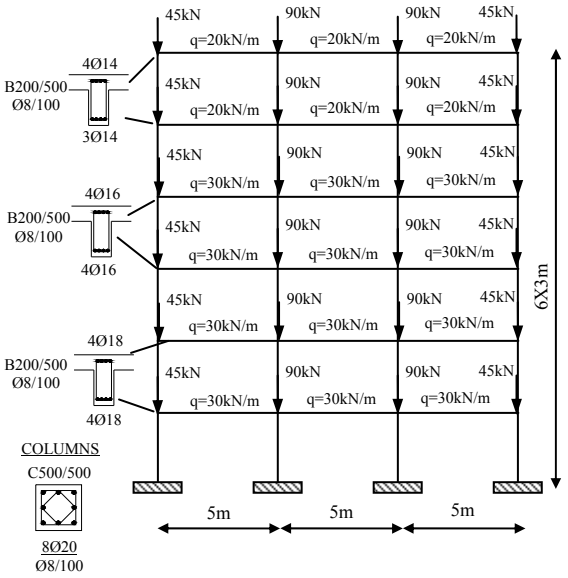

Figure 10. R/C frame layout with flexure-dominated beam members

Fig. 11 illustrates pushover curves derived using the three analytical models for the examined frame. It can be seen that the three models yield insignificant differences in terms of lateral stiffness. However, noticeable variations are observed for the maximum displacement capacities assumed to coincide with the first exceedance of curvature capacity in a base column. Top displacement capacity over building height is predicted as 3.7%, 4.1% and 4.6% by analytical models 1, 2 and 3, respectively.

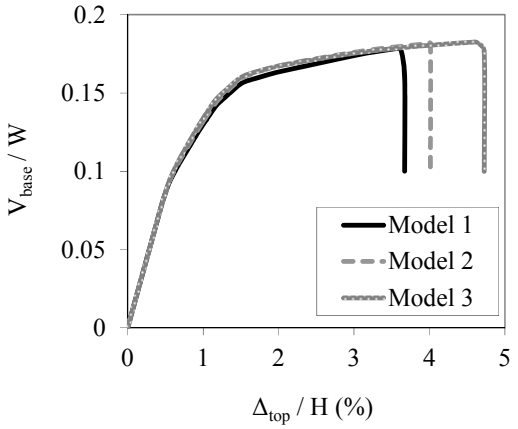

Figure 11. Pushover curves derived using the three different analytical models

Fig. 12a presents column maximum curvature ductility (μ_φ) demands at 3% top drift, which can be considered as a conventional limit for lateral failure (Kappos 1991). These demands are almost identical except for the base columns, where model 1 slightly overestimates μ_φ demand.

In addition, Fig. 12b shows variation of beam maximum μ_φ demands, also at 3% top drift. In contrast with column demands, predicted beam μ_φ demands differ substantially. Higher μ_φ demands are calculated by the proposed analytical model of the present study. Hence, ignoring beam distributed loading may drive the analysis to serious underestimation of end-section curvature demands. The common assumption of linear moment distribution underestimates μ_φ demands at the beam ends subjected

to hogging moments. At these ends, inelastic zone lengths are over-predicted (Fig. 5) and similar rotations are calculated for lower μ_φ demands.

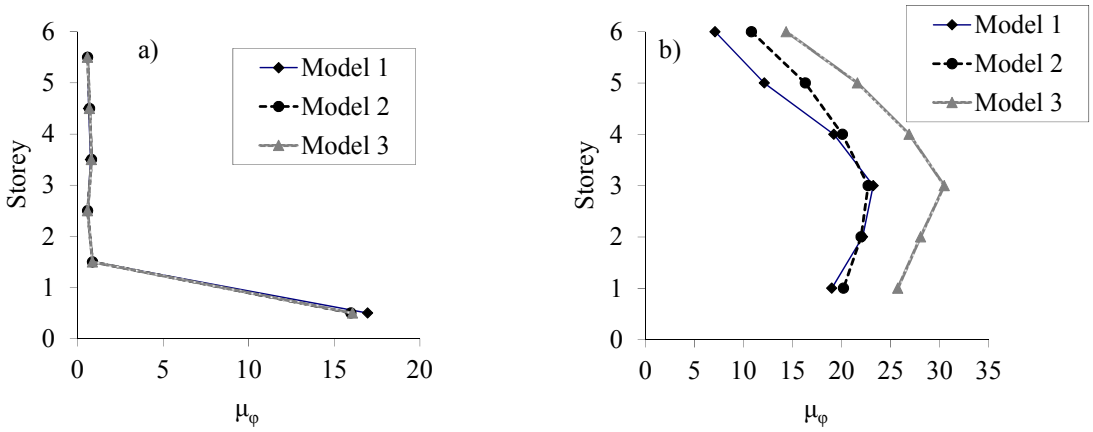

Figure 12. Maximum curvature ductility demands at 3% top drift: (a) columns; (b) beams

This can be seen also in Fig. 13, which illustrates the expansion of flexural inelastic zone coefficient in relation to end section curvature demand for the first story middle beam. Results up to 3% top drift are presented for all applied analytical models. Fig. 13a refers to the beam end subjected to sagging moments and Fig. 13b to the member end developing hogging moments. It is clear that the assumption of linear moment distribution overestimates inelastic zone coefficient and underestimates curvature demand for hogging moments; the opposites hold for sagging moments.

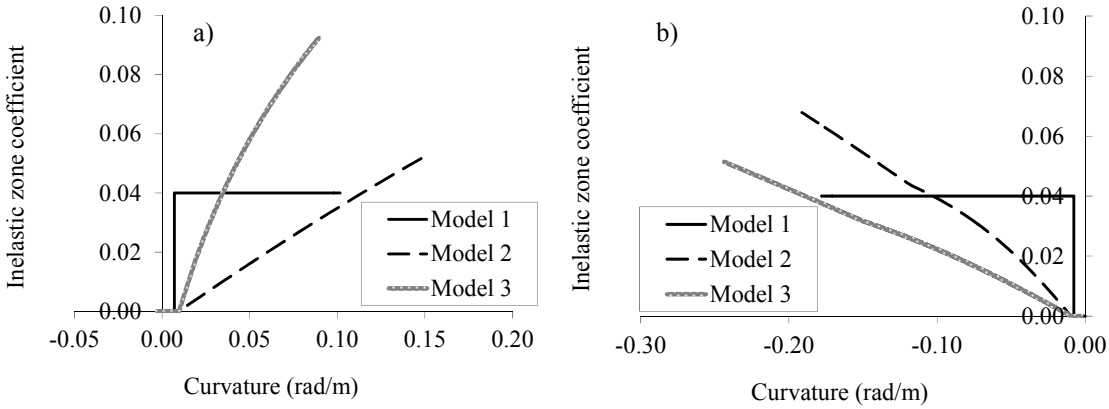

Figure 13. Variation of inelastic zone coefficients with end-section curvature demand for the middle 1st storey beam: (a) sagging; (b) hogging moments

In the following, the response of the R/C frame of Fig. 10 under the near-field ground motion recorded at JMA Kobe Observatory (NS component) with PGA=0.59g is investigated. In particular, Fig. 14a illustrates top displacement history responses derived by the three analytical models. Differences are small, albeit not negligible. Deviations become more significant, when comparing maximum story drifts, shown in Fig. 14b. Model 1 overestimates drift at the lower storeys and underestimates them at the high storeys. Models 2 and 3 predict similar drifts at the first story level, but yield significant deviations at the top two storeys.

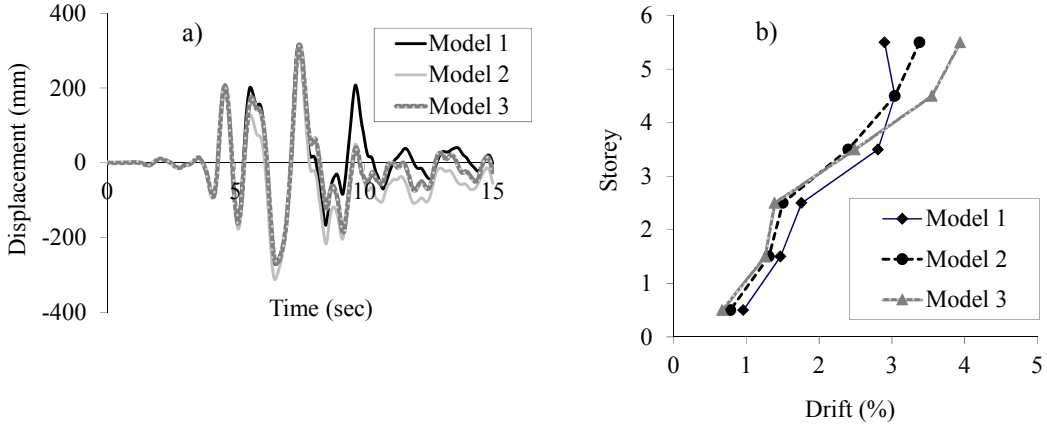

Figure 14. R/C frame responses under JMA Kobe NS component ground motion: (a) top displacement; (b) maximum story drifts

Finally, Fig. 15 shows maximum μ_φ demands derived using the three analytical models for the specific ground motion. It is clear that significant discrepancies are observed for the three analytical models. This points to the need of properly modelling the effect of distributed loading on gradual spreading of inelastic flexural deformations, in the inelastic response history analysis of frame structures.

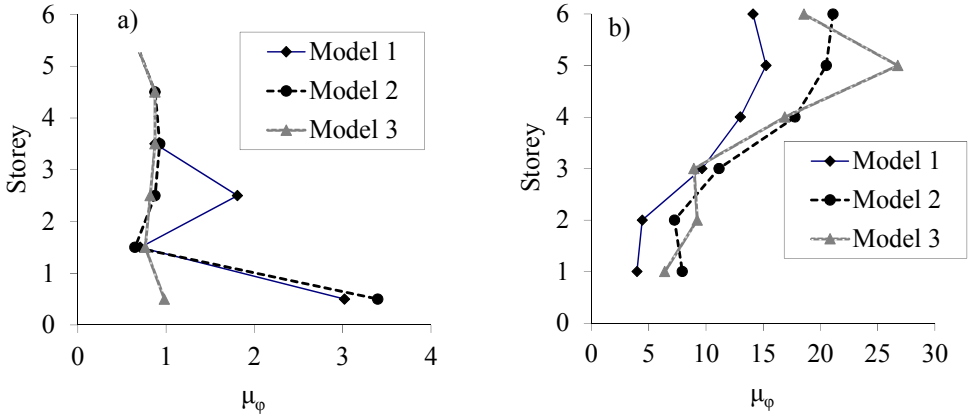

Figure 15. Maximum μ_φ demand predictions under JMA Kobe NS component ground motion: (a) columns; (b) beams

4.2 Portal frame with shear-dominated beam member

The following example, taken from the IDARC2D report (Reinhorn et al. 2009), is a theoretical example intended to demonstrate the program's capability for modelling frame structures with beams yielding in shear. It is a portal frame composed of two columns with similar sectional characteristics and one beam (Fig. 16).

For the two columns, shear deformations can be neglected without loss of accuracy. However, this is not the case for the connecting beam member, which is characterized by low initial shear stiffness GA and limited shear yield capacity V_y. Furthermore, unlike the example included in the IDARC report, the beam member of the frame examined herein is subjected to a uniformly distributed vertical loading q=2kN/m. Hence, the total weight of the frame becomes 48.4kN.

Pushover analysis of this frame is conducted up to the point where curvature demand reaches column curvature capacity φ_u. The beam member does not yield in flexure.

Nevertheless, the beam does yield in shear at its right end. The same is not observed for the left and middle sections of the beam, which remain in the elastic range. The reason for this behaviour becomes evident in Fig. 17a. In this figure, it can be seen that, due to the existence of the distributed loading, shear forces vary along the beam member. In particular, as analysis progresses, shear forces at the three different sections increase in a proportional manner. The constant differences between these lines represent the influence of the distributed loading. In the same figure, it is clear that right section shear force exceeds yield shear at analysis step 530. At the same step, the value of the right shear yielding penetration coefficient (Fig. 17b) begins to increase from zero to 0.46 at the end of the analysis. The latter value agrees well with the middle line of Fig. 17a, which shows that the middle beam section is very close to yielding in shear.

Fig. 18 illustrates pushover curves obtained by three different analytical models for the frame. Model 1 neglects beam shear flexibility. Model 2 accounts for beam shear flexibility. However, distributed loading effect is ignored and shear force is assumed to be constant along the beam member and equal to the actual shear force at the middle section (uniform distributed loading yields zero shear in the middle of the beam). Finally, model 3 is the one proposed in this study.

It is evident that ignoring shear flexibility leads the pushover analysis to serious overestimation of frame lateral stiffness and strength and significant underestimation of displacement capacity. Furthermore, comparing models 2 and 3, it can be seen that the proposed model deviates from model 2, when yielding of the beam right end section occurs. Neglecting gradual spread of inelastic shear deformations by model 2, drives the analysis to considerable overestimation of lateral stiffness and strength and under-prediction of displacement capacity.

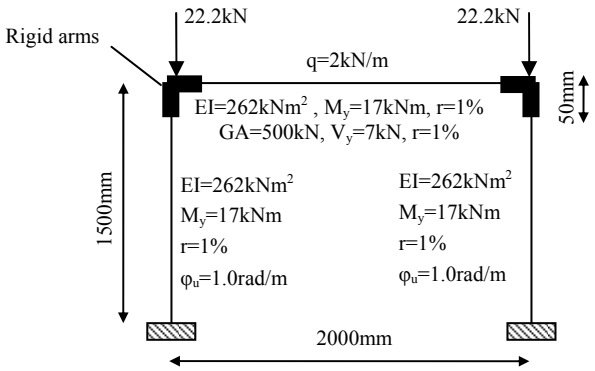

Figure 16. Frame with shear-dominated beam member

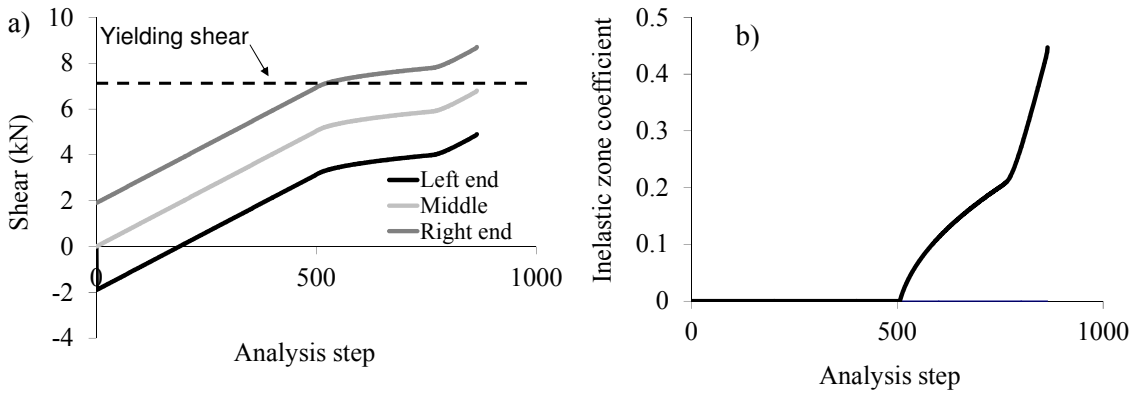

Figure 17. Beam member response: (a) progression of shear forces at different sections; (b) gradual increase of the shear-yielding penetration coefficient

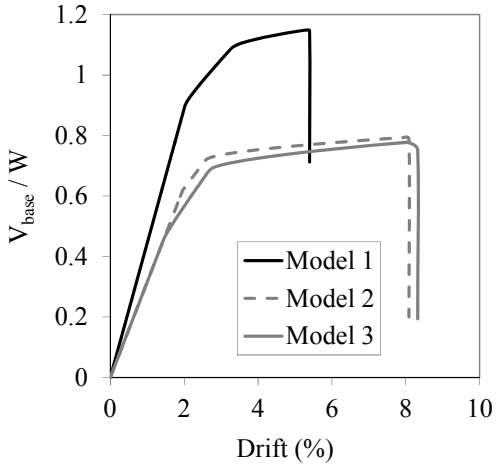

Figure 18. Pushover analysis curves derived by three different analytical models

5. Conclusions

A new gradual spread inelasticity finite element was developed for seismic analysis of beam members with uniform distributed loading. Unlike common inelastic beam elements, the proposed model is able to account consistently for the effect of distributed loading on the variation of flexural and shear stiffness along the beam members throughout their inelastic response. The finite element is accurate for beam members subjected typically to uniaxial bending without axial loading, as well as computationally efficient since it requires monitoring hysteretic response only at the member end sections.

The numerical model was implemented in a general inelastic dynamic analysis finite element code and was used for the analysis of R/C plane frames with beam members dominated either by flexure or shear. It was shown that distributed beam loading effect should be properly and accurately taken into account in the inelastic static and dynamic analysis of frame structures.

References

Anagnostopoulos, S. (1981), "Inelastic beams for seismic analysis of structures", *Journal of Structural Engineering*, **107**(7), 1297-1311.

Addessi, D. and Ciampi, V. (2007), "A regularized force-based beam element with a damage-plastic section constitutive law", *International Journal of Numerical Methods in Engineering*, **70**(5), 610-629.

Beyer, K., Dazio, A. and Priestley, M.J.N. (2011), "Shear deformations of slender R/C walls under seismic loading", *ACI Structural Journal*, **108**(2), 167-177.

Ceresa, P., Petrini, L. and Pinho, R. (2007), "Flexure-shear fibre beam-column elements for modeling frame structures under seismic loading. State of the art", *Journal of Earthquake Engineering*, **11**(1), 46-88.

Clough, R. and Johnston, S. (1966), "Effect of stiffness degradation on earthquake ductility requirements", *Transactions of Japan Earthquake Engineering Symposium,* Tokyo, 195-198.

Filippou, F. and Issa, A. (1988), *Nonlinear analysis of R/C frames under cyclic load reversals*, Report EERC-88/12, Univ. of California Berkeley.

Giberson, M. F. (1967), *The response of nonlinear multi-story structures subjected to earthquake excitation*, Ph.D. thesis, Cal. Tech., Pasadena, California.

Kappos, A.J. (1991), "Analytical Prediction of the Collapse Earthquake for R/C Buildings: Suggested Methodology", *Earthquake Engineering & Structural Dynamics*, **20** (2), 167-176.

Kyakula, M. and Wilkinson, S. (2004), "An improved spread plasticity model for inelastic analysis of R/C frames subjected to seismic loading", *Proc. of the 13th World Conf. Earthquake Engineering*, Vancouver, B.C., Canada.

Lee, C. L. and Filippou, F. (2009), "Efficient beam-column element with variable inelastic end zones", *Journal of Structural Engineering*, **135**(11), 1310-1319.

Lehman, D. and Moehle, J.P. (1998), *Seismic Performance of Well Confined Concrete Bridge Columns*, PEER Report 1998/01, Univ. of California, Berkeley.

Mergos, P.E., and Kappos, A.J. (2008), "A distributed shear and flexural flexibility model with shear-flexure interaction for R/C members subjected to seismic loading", *Journal of Earthquake Engineering and Structural Dynamics*, **37**(12), 1349-1370.

Mergos, P.E., and Kappos, A.J. (2009), "Modelling gradual spread of inelastic flexural, shear and bond-slip deformations and their interaction in plastic hinge regions of R/C members", *Proc. of 2nd COMPDYN Conference*, Rhodes, Greece.

Mergos, P.E. and Kappos, A.J. (2012) "A gradual spread inelasticity model for R/C beam-columns, accounting for flexure, shear and anchorage slip", *Engineering Structures*, **44**, 94-106.

Meyer, C., Roufaiel, S.L. and Arzoumanidis, S.G. (1983), "Analysis of damaged concrete frames for cyclic loads", *Journal of Earthquake Engineering and Structural Dynamics*, **11**(2), 207-222.

Neuenhofer, A. and Filippou, F.C. (1997), "Evaluation of nonlinear frame finite-element models", *Journal of Structural Engineering*, **123**(7), 958-966.

Reinhorn, A.M., Roh, H., Sivaselvan, M., Kunnath, S.K., Valles, R.E., Madan, E., Li, C., Robo, L., and Park, Y.J. (2009), *IDARC2D version 7.0: A program for the inelastic damage analysis of structures,* Tech. Report MCEER-09-0006, State Univ. of New York at Buffalo.

Roh, H., Reinhorn, A.M. and Lee, J.S. (2012), "Power spread plasticity model for inelastic analysis of reinforced concrete structures", *Engineering Structures*, **39**, 148-161.

Sivaselvan, M.V. and Reinhorn, A.M. (2000), "Hysteretic models for deteriorating inelastic structures", *Journal of Engineering Mechanics*, **126**(6), 633-640.

Soleimani, D., Popov, E.P. and Bertero, V.V. (1979), "Nonlinear beam model for R/C frame analysis", *Proc. of 7th Conf. on Electronic Computation*, Struct. Div. ASCE, Washington, 483-509.

Spacone, E., Filippou, F.C. and Taucer, F.F. (1996), "Fiber beam-column model for nonlinear analysis of R/C structures: Formulation", *Journal of Earthquake Engineering and Structural Dynamics*, **25**, 711-725.